J. Math. Biol. (1997) 35: 869–907

Journal of Mathematical Biology

Kinematics of surface growth

R. Skalak[1,2], D. A. Farrow[1], A. Hoger[1,2]

[1]Department of Bioengineering - 0412, University of California, San Diego, La Jolla, CA 92093-0412, USA (e-mail: rskalak@ucsd.edu)
[2]Department of Applied Mechanics and Engineering Sciences, University of California, San Diego, La Jolla, CA 92093-0412, USA

Received 20 February 1996; received in revised form 15 October 1996

Abstract. In this paper a general mathematical framework is developed to describe cases of fixed and moving growth surfaces. This formulation has the mathematical structure suggested by Skalak (1981), but is extended herein to include discussion of possible singularities, incompatibilities, residual stresses and moving growth surfaces. Further, the general theoretical equations necessary for the computation of the final form of a structure from the distribution of growth velocities on a growth surface are presented and applied in a number of examples. It is shown that although assuming growth is always in a direction normal to the current growth surface is generally sufficient, growth at an angle to the growth surface may represent the biological reality more fully in some respects. From a theoretical viewpoint, growth at an angle to a growth surface is necessary in some situations to avoid postulating singularities in the growth velocity field. Examples of growth on fixed and moving surfaces are developed to simulate the generation of horns, seashells, antlers, teeth and similar biological structures.

Key words: Growth – Horns – Shells – Residual stress

1 Introduction

The notion of growth or atrophy of some part of a biological body by the accretion or removal of biological tissue on the surface of the body part is very well established and supported by experimental observations. Tissues that develop by surface growth include bones, nails, horns, antlers and seashells. In some cases, such as nails and horns, the surfaces on which growth occurs are fixed relative to the main structures of the animal (e.g. the skeleton). In other cases, growth takes place on an outer surface, as in seashells and antlers, so that the growth surface itself changes form and position in space relative to the main structures of the animal as growth proceeds.

The term surface growth is used here to denote accretion or removal of material at an external or internal surface of a tissue. In the case of development and remodeling of bones, the cellular mechanisms for augmentation or ablation are described in detail in histological texts (e.g. Fawcett 1994). The development of teeth by surface growth is also well documented (e.g. Moss-Salentijn and Hendricks-Klyvert 1990).

In mathematical and numerical simulations of bone remodeling, it is generally assumed that the surface growth can be described by a growth velocity vector normal to the growth surface (Cowin 1993; Huiskes 1993). While this may be adequate for rounded structures, in some cases of sharp corners, the growth velocity must be considered to be at an angle, not normal, to the growth surface. Further, it is known from anatomical and developmental studies that the generating cells and the new tissue are, often, at an angle to the normal of the growth surface. This is particularly significant in the growth of horns, seashells and teeth as will be shown in subsequent examples.

There is an extensive related literature of pattern formation and morphogenesis which develops patterns and forms by both volumetric and surface growth (e.g. Murray 1989). This literature is based on the use of diffusion–reaction equations as originally suggested by Turing (1952) and developed by Nicolis and Prigogene (1977), Gierer (1981), Koch and Meinhardt (1994) and others. These mathematical descriptions deal mostly with diffusion of morphogens which are extracellular controlling substances. The pattern formation and growth subsequently described does not trace the positional history of individual cells or the extracellular structure generated by a particular cell. In the present study, a more detailed description of the kinematics of surface growth is derived. This theory tracks the cells producing the growth as well as the position and shape of the body generated. Moreover, the curves consisting of material generated by a single cell (called cell-tracks herein) are also part of the description.

There is also a literature of seashell shapes development which essentially generates the external shapes of various existing and fossil seashells by computer algorithms (Illert 1992a, b). This literature is closer to the present paper in concept, but the parameters introduced do not generally correspond to attributes of cell orientation and growth rates producing the three-dimensional forms. The present treatment gives a general theory and some examples of surface growth producing three-dimensional solids (shells, horns, teeth, etc.). The key element in this description is the growth velocities and orientations of the generating cells on the growth surface.

The general formulation for the description of surface growth is developed in Sect. 2 and examples are presented in Sect. 3. Residual stresses that may arise due to surface growth are discussed in Sect. 4. In this regard, the present paper is related to the discussion of compatibility of volumetric growth and associated residual stresses presented in Skalak et al. (1996).

2 Description of surface growth

Consider a body such as shown in Fig. 1A which grows by accretion on an internal or external surface labeled G_0 at $t = 0$ and G at any later time t. The growth surface G may be fixed in space and time relative to some reference cartesian coordinates x_i or it may change its form, size and/or location in space. It is assumed that the new material added at the growth surface G is always on the same side of G, e.g., on the side of the initial region R_0 in Fig. 1A. In this section, it will be assumed that the initial region R_0 is moved as a rigid body due to the surface growth on G, so that at a later time there is a new region R_1 between R_0 and G as shown in Fig. 1B. It is also assumed that the region R_1 and any new material added on G also moves a rigid body. This assumption is not strictly necessary for the main purposes of this paper. Volumetric growth in the region R_1 can be readily incorporated. However, the assumption of rigid body motion of the region R_1 will be relaxed only in Sect. 4 where residual stresses are discussed. Under this assumption, the surface between the regions R_0 and R_1 in Fig. 1B has the same shape as the generating surface G_0 had at $t = 0$, Fig. 1A. To distinguish between the generating cell surface G and the material that is generated on G and is moved away from G, the surfaces which are comprised of material leaving the growth surface at a time $\tau < t$, are designated by H in general. Subscripts 0, τ, t on G and H will be used as necessary to indicate particular times. Thus, H_0 corresponds to G_0, Fig. 1B. Further, we can write $G_t = H_t$, where t is the current time. Note that H_τ ($\tau < t$) has the same shape as G_τ but $H_\tau \neq G_\tau$ in general because H_τ may be in a different position in space.

We take the surface growth to be due to a layer of cells which are located on the surface G and their location on G will be incorporated into the mathematical description. These cells may move with and along the surface

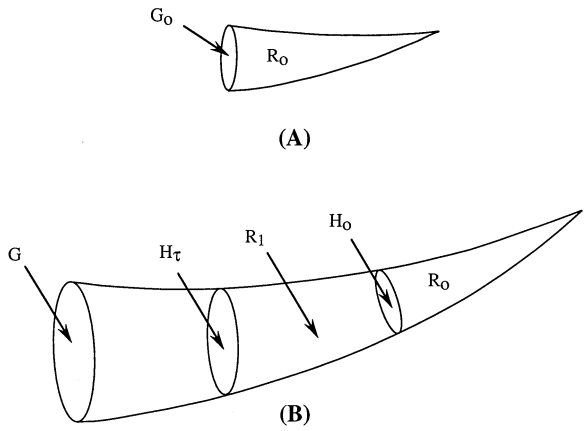

Fig. 1. Nomenclature for surface growth. (A) Initial region R_0 and growth surface G_0 at $t = 0$. (B) New growth, region R_1, and growth surface G at time $t > 0$

G during growth. At each point of G, the rate of growth is defined as the velocity of the material points (which are moved off G due to the material being added) relative to the generating cells on the growth surface itself. This definition of growth velocity $\boldsymbol{v}^g$ defines the growth velocity as a material point velocity and it may be at any angle to the growth surface. If $\boldsymbol{n}$ is a normal to G drawn inward into the region R_1, then when $\boldsymbol{v}^g \cdot \boldsymbol{n} = v_i n_i$ is positive, mass is being added (accretion) and when $\boldsymbol{v}^g \cdot \boldsymbol{n}$ is negative there is removal of mass (ablation). Here and below, bold face symbols indicate vectors (direct notation) and components are indicated by indicial forms, $i = 1, 2, 3$.

A general description of surface growth is conveniently formulated in terms of convected curvilinear material coordinates $(\theta_1, \theta_2, \theta_3)$ by equations of the form

$$x_i = x_i(\theta_1, \theta_2, \theta_3, t) \,, \tag{1}$$

where x_i are fixed, reference cartesian coordinates. The notion of material coordinates θ_i implies that if the θ_i are each held at fixed values, the curve $x_i(t)$ resulting from Eq. (1) describes the path in space of the material point corresponding to the particular set of θ_i values. Equation (1) is assumed to have unique inverse functions

$$\theta_i = \theta_i(x_1, x_2, x_3, t) \tag{2}$$

such that the spatial domain in $\boldsymbol{x}$ occupied by the body at any time has a unique and one to one mapping on a corresponding region of θ-space. The assumptions of continuity and invertibility of Eqs. (1) and (2) excludes some possible cases where there is a point source of volumetric growth and cases in which there is some ablation followed by additional accretion. In the latter case, Eq. (2) may have surfaces on which there are finite discontinuities. To completely define a growing form, the ranges of $\theta_1, \theta_2, \theta_3$ occupied by the body must be known including the location and motion of the cells on the generating surface G at any time, in addition to Eq. (1).

Now two convenient choices of the θ_i will be introduced and retained throughout the rest of this paper. These assumptions are specific choices but they do not restrict the generality of the growth description. They simply make the notation more convenient and compact.

The first choice is to represent the growth surface G as one on which θ_3 is constant (in space) at each instant of time. The value of the constant θ_3 on G may be a function of time, say $f_3(t)$. Then the growth surface is described by

$$\theta_1^G = \theta_1(x_1^G, x_2^G, x_3^G, t) \,, \tag{3}$$

$$\theta_2^G = \theta_2(x_1^G, x_2^G, x_3^G, t) \,, \tag{4}$$

$$\theta_3^G = \theta_3(x_1^G, x_2^G, x_3^G, t) = f_3(t) \,, \tag{5}$$

where x_1^G, x_2^G, x_3^G are cartesian coordinates of points on G and $\theta_i(\boldsymbol{x}, t)$ refers to Eq. (2).

The second choice facilitates a detailed correspondence to the biological reality in cases like seashells, horns and teeth. It is to assume that any pair of values (θ_1, θ_2) held constant on G over any time interval, locates the same physical cell which is producing (extruding) the new growth. The values of $\boldsymbol{x}^G$ for fixed θ_1, θ_2 may change, i.e. the generating cells may move with and along the surface G. At a fixed time, t, a line describing a trajectory through the body which consists of all the particles generated by the same cell is given by

$$\theta_1 = C_2 \,, \tag{6}$$

$$\theta_2 = C_2 \,, \tag{7}$$

$$0 \leqq \theta_3 \leqq f_3(t) \,, \tag{8}$$

where C_1 and C_2 are constants and it is assumed that growth began at $t = 0$, at which time it is also assumed that $\theta_3 = f_3(0) = 0$ for convenience. The curves given by Eqs. (6)–(8) will be called "cell tracks" although they already have specific biological names in some cases such as bivalves and teeth. These will be detailed in the examples in Sect. 3.

As a result of the above choices, the surface defined by

$$x_i = x_i(\theta_1, \theta_2, \tau, t) \,, \tag{9}$$

where τ is a constant in the range $0 \leqq \tau \leqq t$ and t is the current time, is the surface H_τ (Fig. 1B) which is made up of the material points which were generated on surface G_τ at time $t = \tau$.

The velocity of any material point of the extruded body will be designated $\dot{x}_i^m$ where the superscript m denotes a material point. Using Eq. (1),

$$\dot{x}_i^m = \left(\frac{\partial x_i}{\partial t}\right)_{\theta_i} \,, \tag{10}$$

where the subscript θ_i indicates the θ_i variables are held fixed to follow a material particle.

The growth surface $\theta_3 = f_3(t)$ may also be described in terms of its cartesian coordinates x_i^G via Eq. (1):

$$x_i^G = x_i(\theta_1, \theta_2, f_3(t), t) \,. \tag{11}$$

Then the velocity of a generating cell on the surface G having fixed values of θ_1 and θ_2 is given by

$$\dot{x}_i^G = \left(\frac{\partial x_i^G}{\partial t}\right)_{\theta_1,\theta_2} = \left(\frac{\partial x_i}{\partial t}\right)_{\theta_1,\theta_2,\theta_3} + \left(\frac{\partial x_i}{\partial \theta_3}\right)_{\theta_1,\theta_2,t} \frac{df_3}{dt} \,, \tag{12}$$

where x_i and x_i^G refer to Eqs. (1) and (11) respectively. The velocities $\dot{x}_i^G$, Eq. (12), are the velocities of the generating cells on S_t.

Now the growth velocity $\boldsymbol{v}^g$ is defined as the velocity of a material point leaving G relative to the generating cell on G. Thus,

$$v_i^g = \dot{x}_i^m - \dot{x}_i^G \quad \text{on } G \,, \tag{13}$$

where $\dot{\boldsymbol{x}}^m$ refers to the velocity of a material point as it leaves G, Eq. (10). Using Eqs. (10) and (12) in Eq. (13) gives

$$v_i^g = -\frac{\partial x_i}{\partial \theta_3}\frac{df_3}{dt} = v_i^g(\theta_1, \theta_2, t) \quad \text{on } G \tag{14}$$

where the functions $x_i\,(\theta_1, \theta_2, \theta_3, t)$ are those given by Eq. (1) and the derivatives $\partial x_i/\partial\theta_3$ in Eq. (14) are evaluated on G_t. The general case of velocities $\boldsymbol{v}^g$, $\dot{\boldsymbol{x}}^m$ and $\dot{\boldsymbol{x}}^G$ are shown schematically in Fig. 2. If the generating cells on G are assumed to have a long axis, which is parallel to the direction in which they extrude new material (like a tube of tooth paste), then the angle α that $\boldsymbol{v}^g$ makes with the normal $\boldsymbol{n}$ (Fig. 2) is also the inclination of the generating cells with respect to $\boldsymbol{n}$. The new material extruded by the generating cells must, of course, be supplied to them by diffusion or the blood circulation which is not described in the present discussion.

Two special cases using the above vocabulary give simple forms which are useful in particular examples. The first case is that of G being a fixed surface and the generating cells having fixed locations on G. Then $\dot{x}_i^G = 0$ and it follows from Eq. (12) that

$$\left(\frac{\partial x_i}{\partial t}\right)_{\theta_1,\theta_2,\theta_3} = -\left(\frac{\partial x_i}{\partial \theta_3}\right)_{\theta_1,\theta_2,t}\frac{df_3}{dt} \quad \text{on } G. \tag{15}$$

Substituting Eq. (15) in Eq. (14) gives

$$v_i^g = \left(\frac{\partial x_i}{\partial t}\right)_{\theta_1,\theta_2,\theta_3} = \dot{x}_i^m \quad \text{on } G\,, \tag{16}$$

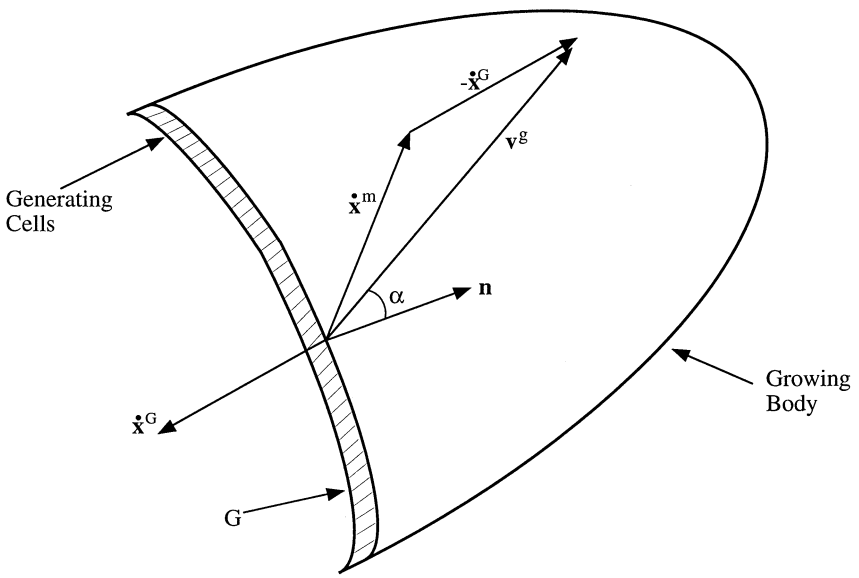

Fig. 2. Schematic diagram of vector velocities at a growth surface. See text for definitions and equations

where $\boldsymbol{x}$ is again given by Eq. (1). Equation (16) corresponds to the logical definition of growth velocity on a fixed surface G, i.e. it is the material point velocity of the material moving away from the fixed surface G.

The second case, in which the extruded material remains fixed in space as a rigid body while the growth surface moves is defined by

$$\dot{x}_i^m = 0 \; . \tag{17}$$

Thus,

$$x_i = x_i(\theta_1, \theta_2, \theta_3) \; . \tag{18}$$

In this case, the motion of the growth surface is given by using Eq. (17) in Eq. (12) so that

$$\dot{x}_i^G = \frac{\partial x_i}{\partial \theta_3} \frac{df_3}{dt} \tag{19}$$

and the growth velocity is, using Eq. (19) in (14),

$$v_i^g = \; - \dot{x}_i^G \; . \tag{20}$$

Equation (20) correctly states that in this case, the growth velocity is the negative of the velocity of the generating cells on G. The negative sign in Eq. (20) is due to the definition of growth velocity as the material point velocity of extruded material relative to generating cells on G.

It is of interest to note that the above vocabulary allows for growth of the cells on G as well as G itself growing. If the cells on G each increase and/or divide and expand their individual cross-sectional area and/or divide and expand on G, then G will also grow in area. This is represented mathematically by the ranges of θ_1 and θ_2 on G being fixed in (θ_i space) but the functions $x_i\,(\theta_i, t)$ in Eq. (1) being adjusted so as to include all the area of the expanding G. The original values of θ_1, θ_2 generate the x_i covering the new G.

On the other hand, if G increases by adding new cells on its periphery, then the ranges of θ_1 and θ_2 on G are expanded (in θ-space). Thus, in the grown body (region R_1 in Fig. 1B) ranges of θ_1 and θ_2 will be functions of θ_3, in this case, since $\theta_3 = f_3\;(\tau) =$ constant represents H_τ corresponding to the time $t = \tau$.

Of course, the mathematical functions can be utilized to allow for growth of the individual generating cells, while allowing for adding new cells at the periphery of G at the same time, by adjusting the ranges of θ_1, θ_2 appropriately.

Division of the generating cells on G cannot be distinguished from expansion of the individual cells on G in the present vocabulary because θ_1 and θ_2 are defined as continuous variables to begin with. A small region of θ_1 and θ_2 space on G may correspond to a single cell at one time. This range may be divided into two parts at any time to simulate cell division. But in the proposed continuum, no separate regions of (θ_1, θ_2) space are identified. The only identification is that a line $\theta_1 = C_1$, $\theta_2 = C_2$, always represents material from the same cell, without regard to the extent of the cell in a plane normal to

this line. There are in principle, an infinite number of such lines (cell tracks) emanating from any G_t or any part of it.

It may be noted that the mathematical description proposed above is new insofar as it describes both the growth velocity and cell tracks as well as the motion of G and the motion and growth of generating cells on G. Most previous treatments of surface growth assume only normal growth velocities, which are generally sufficient to describe the rate of addition of mass and the change of body form, but do not allow for definition of realistic cell tracks or the explicit growth and motion of generating cells on G.

The cell tracks defined by Eqs. (6)–(8) are the same in concept to streak lines defined in fluid mechanics. A streak line consists of points in a fluid which at some previous time, passed through the same fixed point in space, like a smoke line from a fixed source. Cell tracks are similar but different in that source points (generating cells) may move in space. Cell tracks are like smoke lines generated by a moving point source.

The surfaces H_τ (Fig. 1B) defined by Eq. (9) are the same, in concept, to time lines defined in fluid mechanics. A time line is made up of points in a fluid which at some earlier time were all located along a given straight line. The generating surface H_τ consists of points all generated at an earlier time $\tau < t$, but the generating surface is not a line and generally not plane. In a fluid, time lines usually deform as time progresses. In the present theory growth surfaces H_τ do not change form with time, but must move as rigid bodies.

Material particle paths in the present vocabulary have the same definition and physical meaning as in fluid mechanics and solid mechanics. Particle paths may or may not be different from cell tracks, just as particle paths and streak lines may or may not be the same in fluid mechanics.

Stream lines may also be defined in the present theory using exactly the same definition and physical interpretation as in fluid mechanics. Stream lines are curves which are everywhere tangent to the instantaneous material velocities. They are useful to visualize the instantaneous pattern of mass flow.

Under the assumption that the growing body moves as a rigid body, the growth velocity $\boldsymbol{v}^g$ and the motion of the growth surface $\dot{\boldsymbol{x}}^G$ must be such that (see Eq. (13)):

$$\dot{\boldsymbol{x}}^m = \boldsymbol{v}^g + \dot{\boldsymbol{x}}^G = \boldsymbol{u} + \boldsymbol{w} \times \boldsymbol{x} \,, \tag{21}$$

where the vectors $\boldsymbol{u}$ and $\boldsymbol{w}$ are not functions of $\boldsymbol{x}$, but may depend on time and $\boldsymbol{w} \times \boldsymbol{x}$ indicates the cross-product. The form of $\boldsymbol{v}^g$ in Eq. (21) is the same as that of Volterra dislocations which are also relative motions of two rigid surfaces.

A problem of theoretical and biological interest is to construct the descriptions of growth of the form of Eq. (1) when the growth velocities $\boldsymbol{v}^g$, Eq. (14) and the growth surface G, Eq. (11), are given. When G is a rigid surface and the generating cells are fixed on it, it will usually be convenient to express $\boldsymbol{v}^g$ via the functions $\boldsymbol{u}(t)$ and $\boldsymbol{w}(t)$ in Eq. (21) and to compute the resulting forms which may then be compared to the biological forms and cell tracks in animals.

In the case that G is fixed and $\dot{\boldsymbol{x}}^G = 0$ in Eq. (21), and $\boldsymbol{u}$ and $\boldsymbol{w}$ are given, it is possible to construct an integral equation which describes the resulting body form. Assume that the growth starts from the known G_0 at $t = 0$. Any curvilinear coordinates θ_1, θ_2 on G_0 at $t = 0$ may be assigned in the form

$$\theta_1 = f_1(x_i^0), \qquad \theta_2 = f_2(x_i^0) \tag{22}$$

where x_i^0 are cartesian coordinates on G_0.

Now at $t = 0$,

$$\boldsymbol{v}^m = \boldsymbol{u} + \boldsymbol{w} \times \boldsymbol{x}^0 \quad \text{on } G\,, \tag{23}$$

where $\boldsymbol{x}^0$ denotes coordinates on G. After a time interval Δt, the mass particle generated at $\boldsymbol{x}^0$ will have the coordinates $\boldsymbol{x}$ where

$$\boldsymbol{x} = \boldsymbol{x}^0 + \boldsymbol{v}^m \Delta t = \boldsymbol{x}^0 + (\boldsymbol{u} + \boldsymbol{w} \times \boldsymbol{x}^0)\,\Delta t\,. \tag{24}$$

It follows by tracing successive time increments, Δt, that the location of a material point identified by fixed θ-values is given in general by the integral equation

$$\boldsymbol{x}(\theta, t) = \boldsymbol{x}^0(\theta_1, \theta_2) + \int_{\tau_0}^{t} [\boldsymbol{u}(\tau) + \boldsymbol{w}(\tau) \times \boldsymbol{x}(\theta, \tau)]\, d\tau \tag{25}$$

where τ_0 is the time at which the particle is first generated on G. For simplicity and without loss of generality, we may take $f_3(t) = t$ in Eq. (5) so $\tau_0 = \theta_3$. Integration of Eq. (25) then yields the general description of the growth in the form of Eq. (1).

If G is not a surface of fixed form, but the body generated moves as a rigid body, it is convenient to choose the reference axis $\boldsymbol{x}$ as fixed to the growing body so only the suface G moves. This is a convenient mode of description of the growth of shells, bones and antlers which are regarded as rigid bodies in the present approximation and grow by deposition of material on the surface G which is always part of the external surface of the body. The generating cells may move with and on the surface G leaving the new material behind them. There is no constraint for compatibility in this case, i.e. $\boldsymbol{v}^g$ can be any continuous vector function over G and is not restricted to rigid body motions.

If $\boldsymbol{v}^g$ is specified on G as a function of (θ_1, θ_2, t) (in reality $\boldsymbol{v}^g$ is controlled for any fixed θ_1, θ_2, i.e. for a particular cell, by a genetic code and environmental influences), but Eq. (1) are not given, we may reconstruct the body generated by the following process.

Assume G_0 is known, and the initial coordinates $\boldsymbol{x}_i^0$ on G are

$$x_1^0 = x_1^0(\theta_1, \theta_2), \quad x_2^0 = x_2^0(\theta_1, \theta_2), \quad x_3^0 = x_3^0(\theta_1, \theta_2) \quad \text{at } t = 0\,, \tag{26}$$

where the superscript 0 indicates these are values on G_0 at $t = 0$. The case here corresponds to Eqs. (17)–(20) so that

$$\dot{x}_i^G = -\,v_i^g(\theta_1, \theta_2, t)\,. \tag{27}$$

Holding θ_1, θ_2 constant, the integration of Eq. (27) with the initial conditions (26) yields the trajectory of the cell on G with coordinates θ_1, θ_2:

$$x_i^G(\theta_1, \theta_2, t) = x_i^0(\theta_1, \theta_2) + \int_0^t (-v_i^g(\theta_1, \theta_2, \tau)\, d\tau\,. \tag{28}$$

At this point, it is of interest to note that in a typical problem of producing a sequence of surfaces G, there may be various different vector growth velocities $\boldsymbol{v}^g$ which produce the same set of surfaces G. But these will not have the same cell tracks, as indicated in the schematic examples shown in Fig. 3A, B. In Fig. 3A, all $\boldsymbol{v}^g$ are parallel. In Fig. 3B, all growth vectors are normal to the initial G. If the surfaces G at different times are smooth and $\boldsymbol{v}^g$ is a continuous distribution, then the successive G surfaces can always be produced by a distribution of $\boldsymbol{v}^g$ which is always normal to the current G. This is what is usually assumed in studies of bone growth and atrophy due to stress (Cowin 1993; Huiskes et al. 1994).

It should be noted that the rate at which mass is created per unit area on G is always given by

$$\dot{m} = \rho \boldsymbol{v}^g \cdot \boldsymbol{n}\,, \tag{29}$$

where $\boldsymbol{n}$ is the normal to G ($\boldsymbol{n}$ is taken positive when pointing into the tissue being created) and ρ is the density of the new growth or that of tissue being removed, when $\boldsymbol{v}^g \cdot \boldsymbol{n}$ is negative. Any two distributions of $\boldsymbol{v}^g$ which produce the same sequence of surfaces G must have the same normal component of growth velocity. There usually exists a purely normal distribution of $\boldsymbol{v}^g$ to

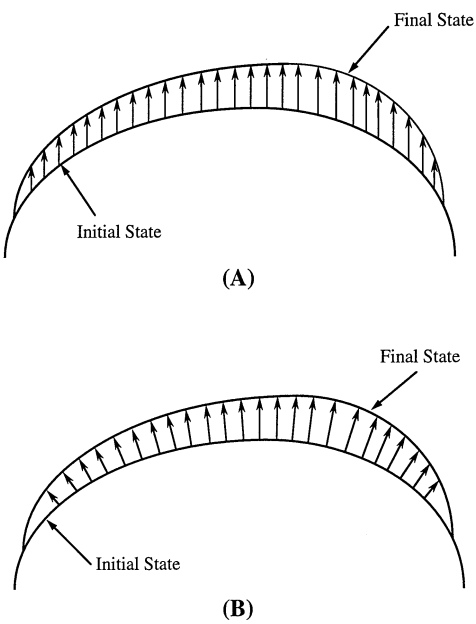

Fig. 3. Illustration of how the same final surface may be produced by different growth velocities. (A) All growth velocities are parallel to each other. (B) All growth velocities are normal to the growth surface

describe the rate of mass addition and the sequence of surfaces G. But purely normal growth may not suffice to describe the biological cell tracks observed in vivo. It may also not lead to a realistic description of singular points on the growth surface, as discussed below.

In the case of a sharp corner to be created at an angle α to G, as shown in Fig. 4A, growth in the normal direction cannot produce the required form without a singular growth velocity. The discussion is simplified by reverting to the case of G being fixed on the x_1 axis and generating the region R_1, Fig. 4A, whose outer boundary is at the angle α to the x_1, x_3 plane. Figure 4B shows the normal velocity distribution that can produce part of the region R_1 (the part DEHG). But the blank part (EHF) cannot be produced by growth normal to G. It would require a point source at E to fan out and produce the region EHF. This would be a singularity at E and require a *deformation* rather than rigid body motion of the region EHF as time progressed which is not physiological. In the growth of some horns, teeth and seashells it is known that the generating cells are, in fact, oriented at an angle to G, as shown in Fig. 4C.

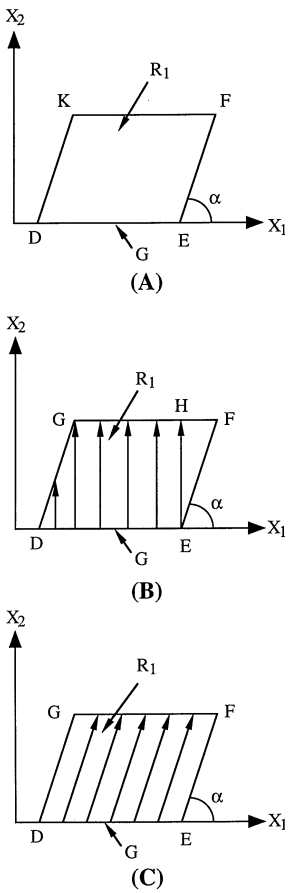

Fig. 4. (A) Schematic diagram of a region R_1 growing at angle α to the growth surface G. (B) Growth produced by growth velocities normal to G. Region EHF cannot be produced. (C) Growth produced by growth velocities at angle α to G

3 Examples of surface growth

The following examples are chosen to illustrate growth from fixed and changing surfaces, starting with elementary examples to illustrate general principles and proceeding to more realistic biological cases.

Example 3.1. Fixed growth surface

Suppose G is a fixed circular area in the x_1, x_2 plane, centered at the origin with radius a as shown in Fig. 5. Further, suppose that $\boldsymbol{v}^g$ is given as a constant vector over G:

$$\boldsymbol{v}^g = v_0 \boldsymbol{i}_3 \,, \tag{30}$$

where v_0 is a constant and $\boldsymbol{i}_3$ is a unit vector in the x_3 direction. Assume the generating cells on G are fixed in position. Then choose $\theta_1 = x_1$, $\theta_2 = x_2$ and $\theta_3 = \tau$ where τ is the time at which any material point is first generated.

In this case Eq. (25) gives

$$\boldsymbol{x} = \boldsymbol{x}^0 + \int_{\theta_3}^{t} v_0 \boldsymbol{i}_3 \, d\tau = \boldsymbol{x}^0 + v_0 (t - \theta_3) \boldsymbol{i}_3 \,. \tag{31}$$

Equation (31) gives the components

$$x_1 = \theta_1, \quad x_2 = \theta_2, \quad x_3 = v_0 (t - \theta_3) \,. \tag{32}$$

Equation (32) is the explicit expression of Eq. (1) for this case and is valid in the domain $\theta_1^2 + \theta_2^2 \leqq a^2$ and $0 \leqq \theta_3 \leqq t$. The grown length is $L = v_0 t$. The particle paths and cell tracks are the same set of straight lines as shown in Fig. 5.

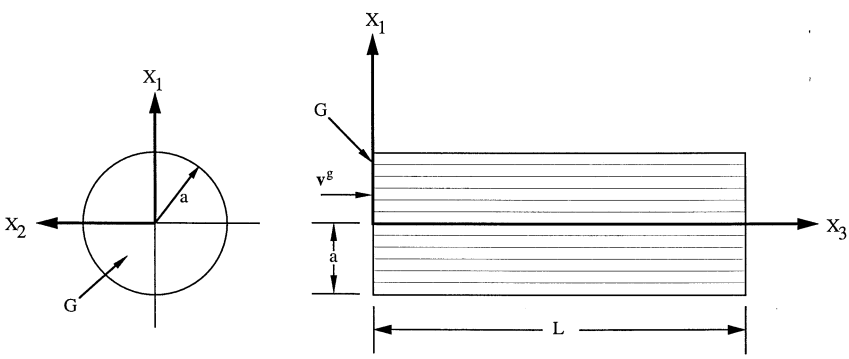

Fig. 5. Growth of a cylinder from a fixed growth surface G

Example 3.2. Growth surface accreting on edges

Consider a case in which G is again a circular area fixed at $x_3 = 0$, but with a radius "a" which grows so that

$$a = kt \,, \tag{33}$$

where k is a constant. Suppose the growth velocity is again given by Eq. (30). Then with the same choices of θ_i as in Example 3.1, Eqs. (31) and (32) also hold here. The only difference is that the domain in θ space is now limited to $(\theta_1^2 + \theta_2^2) \leqq k^2\theta_3^2$ and $0 \leqq \theta_3 \leqq t$. The solution implies that the cells on G are fixed in position once they are generated and new cells are added at the periphery of G as G grows. The solid generated is a cone with half angle γ where $\tan\gamma = k/v_0$ and all cell tracks and particle paths are lines parallel to x_3 as shown in Fig. 6.

Example 3.3. Growth surface accreting with varying $\boldsymbol{v}^g$

Consider next a problem in which the external shape is given to be the same as the cone in Example 3.2, Fig. 6, but with the cell tracks as shown in Fig. 7. The cone in Fig. 7 grows exactly at the same rate as in Fig. 6 so $L = v_0 t$ and $a = kt$ in Fig. 7 and the cone half-angle is again γ where $\tan\gamma = k/v_0$. The motivation for Fig. 7 is that cell tracks may be the direction of the final fiber structure and the fiber directions shown in Fig. 7 may produce a stronger structure than those in Fig. 6.

The interior cell tracks in Fig. 7 form cones with half-angles β where $0 \leqq \beta \leqq \gamma$. The vector field $\boldsymbol{v}^g$ must also be such that $\boldsymbol{v}^g \cdot \boldsymbol{n} = v_0$ on G to supply the mass required. At the same time there must be a radial velocity inwards at angle β to $\boldsymbol{i}_3$ to produce the inclination of the cell tracks. The distribution of $\boldsymbol{v}^g$ on $x_3 = 0$ satisfying these conditions is

$$\boldsymbol{v}^g = -\frac{x_3}{t}\boldsymbol{i}_1 - \frac{x_2}{t}\boldsymbol{i}_2 + v_0\boldsymbol{i}_3 \,. \tag{34}$$

The results given by Eq. (34) is derived using the fact that the values of θ_1 and θ_2 are constant on cell tracks. The values of θ_1 and θ_2 on the surface of the cone with half-angle β are assigned to be $\theta_1 = \beta\cos\phi$ and $\theta_2 = \beta\sin\phi$. From the geometry of Fig. 7, it can be shown that for any time, t, and position $\boldsymbol{x}$ that

$$\theta_1 = \beta\frac{x_1}{r} \,, \tag{35}$$

$$\theta_2 = \beta\frac{x_2}{r} \,, \tag{36}$$

$$\theta_3 = t - \frac{x_3}{v_0} \,, \tag{37}$$

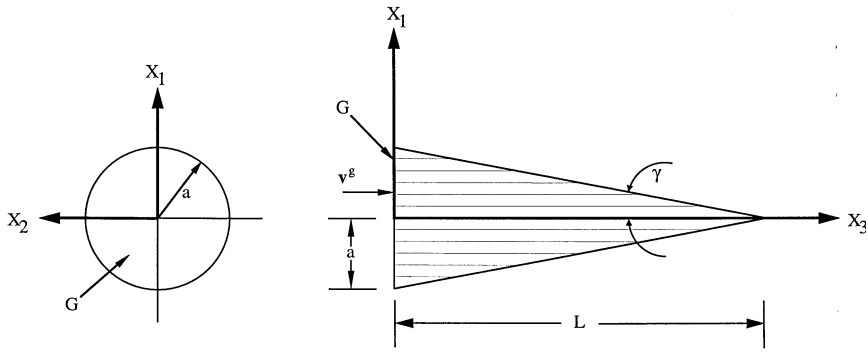

Fig. 6. Growth of a cone by normal growth velocities on an expanding growth surface G

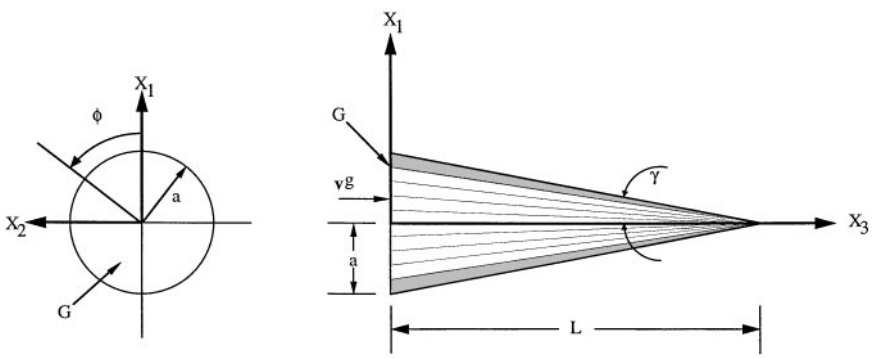

Fig. 7. Growth of a cone from an expanding surface G by growth velocities at variable angles to the growth surface to produce the cell tracks shown

where β and r are given by

$$\beta = \tan^{-1}\left(\frac{r}{v_0 t - x_3}\right) \tag{37a}$$

and

$$r = [x_1^2 + x_2^2]^{1/2} \tag{37b}$$

so that Eqs. (35)–(37) give θ_i in terms of x_i and t.

Equations (35)–(37) can be inverted to give

$$x_1 = v_0 \frac{\theta_3 \theta_1}{\beta} \tan \beta \,, \tag{38}$$

$$x_2 = v_0 \frac{\theta_3 \theta_2}{\beta} \tan \beta \,, \tag{39}$$

$$x_3 = v_0(t - \theta_3) \,, \tag{40}$$

where now

$$\beta = [\theta_1^2 + \theta_2^2]^{1/2} \,, \tag{41}$$

so that Eqs. (38)–(40) give x_i in terms of θ_i and t. It follows from Eqs. (38)–(40) and Eqs. (10) that

$$\dot{x}_1^m = 0, \qquad \dot{x}_2^m = 0, \qquad \dot{x}_3^m = v_0 \,. \tag{42}$$

Equation (42) shows that the particles move in straight lines parallel to $\boldsymbol{i}_3$, as expected. Note that in this case the particle paths are not the same as the cell tracks shown in Fig. 7.

It also follows from Eqs. (38)–(40) and Eq. (12) that

$$\dot{x}_1^G = \frac{x_1}{\theta_3} = \frac{x_1}{t} \,, \tag{43}$$

$$\dot{x}_2^G = \frac{x_2}{\theta_3} = \frac{x_2}{t} \,, \tag{44}$$

$$\dot{x}_3^G = 0 \,. \tag{45}$$

The result shown in Eqs. (43) and (44) is a result of the self-similarity of cones and is not expected to generalize to other shapes. Using Eqs. (43)–(45) and (42) to compute $\boldsymbol{v}^g$ by substituting into Eq. (13) gives exactly the vector field of Eq. (34), which demonstrates the consistency of the solution.

Also note that the cells on G move radially outward with radial velocity $v_0 \tan\beta$, as time increases as indicated by Eqs. (43) and (44) and G must increase in area as time increases. If the range of θ_1, θ_2 is terminated at some angle γ_1 where $\gamma_1 < \gamma$, a hollow horn is generated as indicated by the stippled area in Fig. 7.

Example 3.4. Axes fixed relative to the growing body

Consider the same cone structure and growth as shown in Fig. 7, but viewed from axis $\boldsymbol{x}$ which are fixed to the growing body. In this case, the growth surface G moves to the left at velocity $(-v_0)$ as shown in Fig. 8. The length of

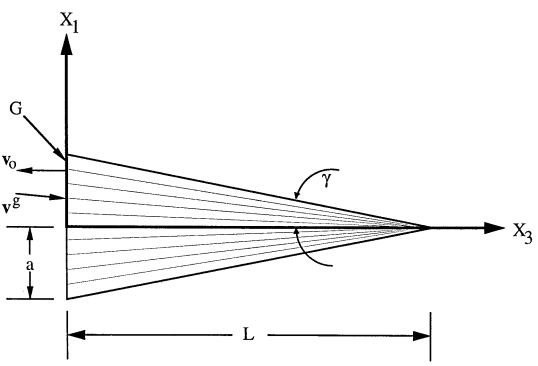

Fig. 8. Growth of the same cone as in Fig. 7, but viewed from axes fixed to the cone so that the growth surface moves to the left at velocity v_0

the cone is $L = v_0 t$, the radius of G is $a = kt$, and the cone half-angle is γ where $\tan \gamma = (k/v_0)$, as in Fig. 7. Equation (1) describing the growth in Fig. 8 is obtained from Eqs. (38)–(40) by replacing x_3 by $(x_3 + v_0 t)$. Then x_1 and x_2 are again given by Eqs. (38) and (39), but Eq. (40) changes to $x_3 = -v_0 \theta_3$. It can be readily shown that $\boldsymbol{v}^g$ is again given by Eq. (34), but now $\dot{\boldsymbol{x}}^m = 0$ and $\dot{\boldsymbol{x}}^G = -\boldsymbol{v}^g$. The physical interpretation is now that the cells on G are moving along the cell tracks that they are generating and leaving the new material behind them at rest. It is noteworthy that in the Examples 3.3 and 3.4 that the vector growth velocity $\boldsymbol{v}^g$ is independent of the reference system $\boldsymbol{x}$, as it should be when properly defined.

Example 3.5. A curvilinear horn

Let G be a circle in the (x_2, x_3) plane centered at $(0, -r_0, 0)$ as shown in Fig. 9B. The radius a of G is specified as

$$a = a_0 \frac{2k}{\pi} t \,, \tag{46}$$

where a_0 and k are constants. On G a growth velocity is specified as

$$\boldsymbol{v}^g = -kx_2 \boldsymbol{i}_1 \,. \tag{47}$$

The problem is to find the resulting shape grown. The answer is shown (at time $t = \pi/2k$) in Fig. 9A. It is a horn with a circular center line. To show this, we proceed as follows.

Note that $\boldsymbol{v}^g$ is of the form of Eq. (21) with $\boldsymbol{u} = 0$ and $\boldsymbol{w} = k\boldsymbol{i}_3$. Since G is fixed in the (x_2, x_3) plane, Eq. (25) is applicable and gives an integral equation for the cell tracks $(\theta_1, \theta_2) =$ constants. Values of (θ_1, θ_2) are chosen on G as shown in Fig. 9B:

$$\theta_1 = x_2^G + r_0, \qquad \theta_2 = x_3^G. \tag{48}$$

The integral equation (25) becomes

$$\boldsymbol{x}(\theta, t) = \boldsymbol{x}^G(\theta_1, \theta_2) + \int_{\tau_0}^{t} (k\boldsymbol{i}_3) \times \boldsymbol{x}(\theta, \tau)\, d\tau \,, \tag{49}$$

where τ_0 is the time that growth begins at (θ_1, θ_2) i.e. when this point becomes part of the growth surface. Consider the point $(0, -r_0, 0)$ at which growth starts at $t = 0$. For this point, the components of Eq. (49) are the pair of integral equations for x_1 and x_2:

$$x_1 = -\int_0^t kx_2(\tau)\, d\tau \,, \tag{50}$$

$$x_2 = -r_0 + \int_0^t kx_1(\tau)\, d\tau \,. \tag{51}$$

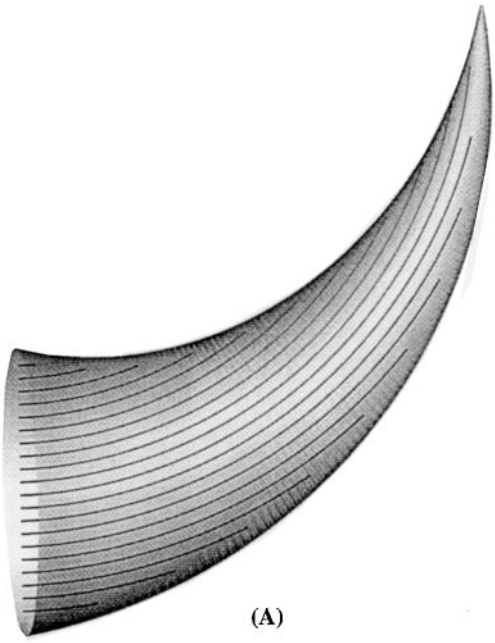

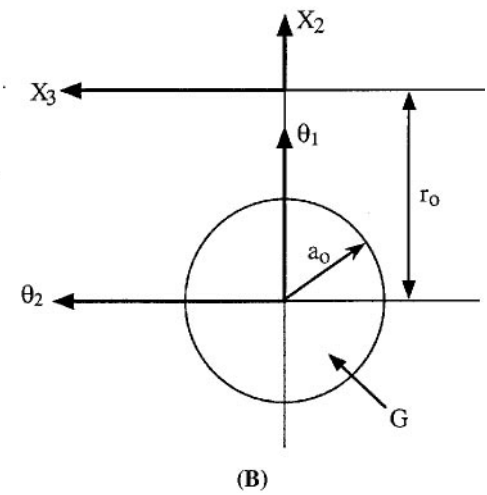

Fig. 9. A horn grown from expanding surface *G*. All cell tracks shown are segments of concentric circles

The solution to Eqs. (50) and (51) is

$$x_1 = r_0 \sin kt \ , \tag{52}$$

$$x_2 = -r_0 \cos kt \ . \tag{53}$$

Equations (52) and (53) show that the centerline of the horn is part of a circle, as shown in Fig. 9A. In a similar manner, it can be shown that every cell track (and particle path) for this $\boldsymbol{v}^g$ is part of a circle with radius $(r_0 - \theta_1)$, Fig. 9B. Further, the angular velocity of each particle with respect to the x_3 axis is k since $\boldsymbol{w} = k\boldsymbol{i}_3$.

The horn developed is shown in Fig. 9A at time $t = (\pi/2k)$ when the centerline is a quarter circle and the radius of G is a_0. The coordinate θ_3 is again taken to be $\theta_3 = \tau$ where τ is the time at which a particular particle is initiated on G. Then $\theta_3 =$ constant, is a plane containing the x_3 axis. Several such planes are shown in Fig. 9B. In each such plane, the cross-section of the horn will be a circle.

Example 3.6. A curvilinear horn of logarithmic spirals

Consider producing a horn with the external form shown in Fig. 9, but with cell tracks which are at constant angles to the centerline, similar to Fig. 8, as compared to Fig. 6. This may be accomplished by the use of logarithmic spirals which are extensively discussed by D'arcy Thompson (1942) in connection with the forms of shells, horns and other biological forms. Logarithmic spirals are plane curves (Fig. 10) described by

$$r = b\mathrm{e}^{\theta \cot \alpha}, \tag{54}$$

where r, θ are polar coordinates and b and α are constants. The angle between the tangent to the spiral and the radius vector $\boldsymbol{r}$ is the constant angle α. This property is suggested in the alternate name of equiangular spiral. If α is $< 90^\circ$, then r increases with θ. If α is $> 90^\circ$, then r decreases with θ, i.e. the curve spirals inwards rather than outwards. When $\alpha = 90^\circ$, r is constant and the spiral becomes a circle.

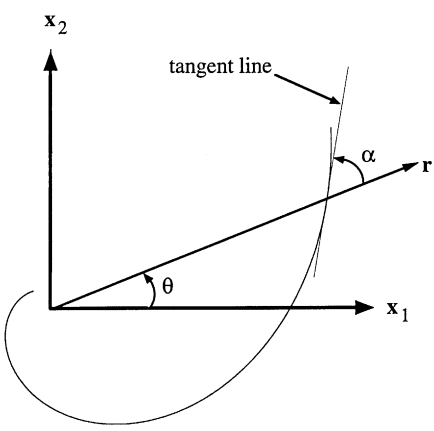

Fig. 10. A logarithmic spiral. The angle α between the tangent to the spiral and the radius vector $\boldsymbol{r}$ is constant

In Fig. 11, a close approximation to the boundaries shown in Fig. 9 are illustrated for a specific case. Fig. 11 is a cross-section of a horn with the following logarithmic spirals as the cell tracks. The problem to be solved is to find the growth velocity $\boldsymbol{v}^g$ that produces this horn.

From Table 1 it can be seen that the center-line curve C_0 is a circle. The curves C_1 and C_2 are logarithmic spirals which spiral outwards. The curves C_3 and C_4 are logarithmic curves spiraling inwards. The constants in Table 1 have been adjusted so that all curves meet at the point (50, 0) so C_0 is a quarter of a circle.

The cross-section shown in Fig. 11 is the curved counterpart of Fig. 8 in the sense that along any radius in Fig. 11 the angle between tangents to the curves C_0, C_1, C_2, C_3, C_4 are constants independent of θ. The same is true for

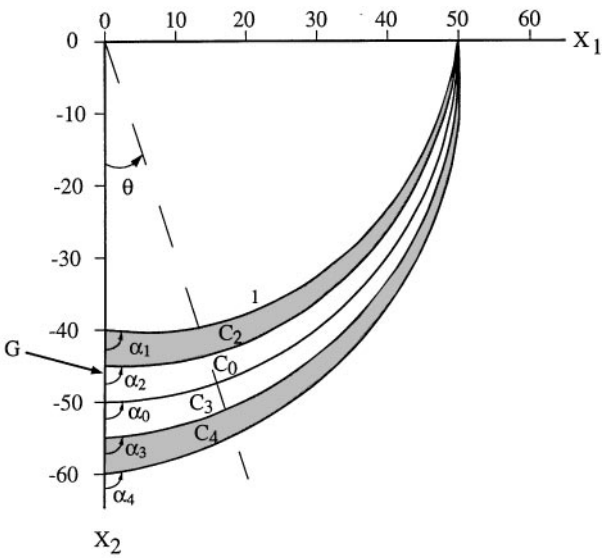

Fig. 11. A horn grown from an expanding surface G by growth velocities at various angles to G to produce logarithmic spiral cell tracks as shown. The centerline is a segment of a circle

Table 1. Dimensions and constants of cell tracks in Fig. 11

Curve	b (cm)	α (deg)
C_1	40	81.92
C_2	45	86.34
C_0	50	90.00
C_3	55	93.47
C_4	60	96.62

the cell tracks in Fig. 8, for any line drawn parallel to the x_1 axis (which is the analogue of r as $r \to \infty$).

To complete the description of the 3-D horn, whose section is shown in Fig. 11, we assume that G is always a circle, and that as a result, sections $\theta_3 =$ constant, are planes containing the x_3 axis. The cross-sections on such planes are then also circles. Curves on which $(\theta_1^2 + \theta_2^2) =$ constant, are also circles in the interior on $\theta_3 =$ constant planes. The stipulation that G is always a circle, together with the two cell tracks C_1 and C_4, completely defined the external geometry of the horn. The cell tracks in the interior in Fig. 11 are defined by requiring them to be logarithmic spirals. Cell tracks which are not in the plane shown in Fig. 11, must have some component of the growth velocity in the x_3 direction as well as in the x_1, x_2 plane. The information given above is sufficient to develop a computer program based on Eq. (25) which generates this 3-D horn. A computer drawn 3-D view of the horn is shown in Fig. 12.

Logarithmic spirals were extensively discussed by D'arcy Thompson (1942), primarily with respect to shells in which the spiral angle is constant for all points of the shell. The use of inward and outward spirals for horns as in Fig. 11 was not developed.

In Fig. 11, the stippled area indicates a possible cross-section of a hollow horn. The solid tip may be produced by a change of G from a circle to a ring as growth proceeds as shown schematically in Fig. 13.

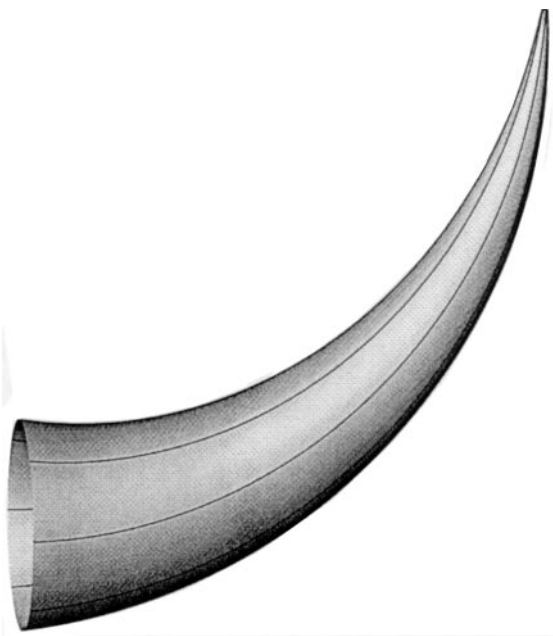

Fig. 12. Computer generated 3-D-view of the horn shown schematically in Fig. 11

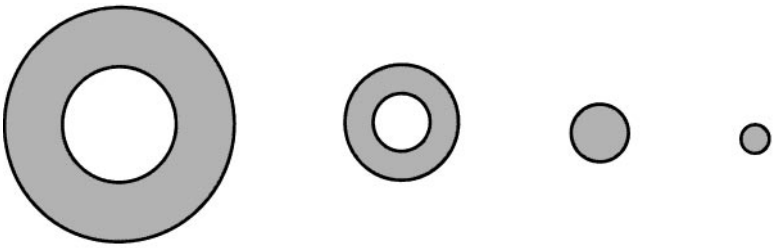

Fig. 13. Regions of active growth on growth surface G (stippled areas) to produce a hollow horn such shown stippled in Fig. 11

Example 3.7. A curvilinear horn of flatter spirals

Another example of growth of a horn is illustrated in Fig. 14. In this example, no cell track is a circle, but all cell tracks are flat logarithmic spirals, similar to a long-horn steer. Here the parameters in Eq. (54) are chosen as follows.

The values in Table 2 produce the curves starting at A and B in Fig. 14. To define the rest of the horn, planes are chosen so that they intersect the curves C_1 and C_2 at equal angles. In this $\beta_1 = \beta_2 = 82.10^\circ$ in Fig. 14. Such surfaces are assumed to be generating surfaces and the cross-sections of the horn on such planes are assumed to be circles H_τ which were on the generating surface G_τ at earlier times.

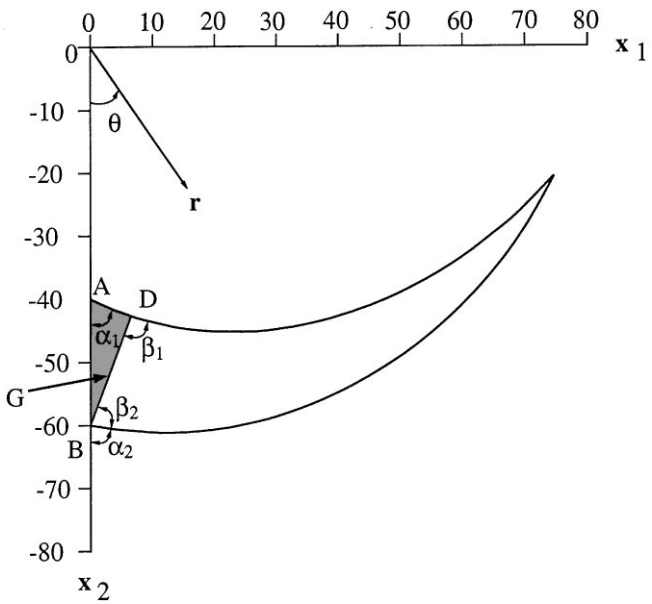

Fig. 14. A horn grown from an expanding surface G by growth velocities such that all cell tracks are expanding logarithmic spirals

Table 2. Dimensions and constants of cell tracks in Fig. 14

Curve	b (cm)	α (deg)
C_1	40	63.01
C_2	60	78.81

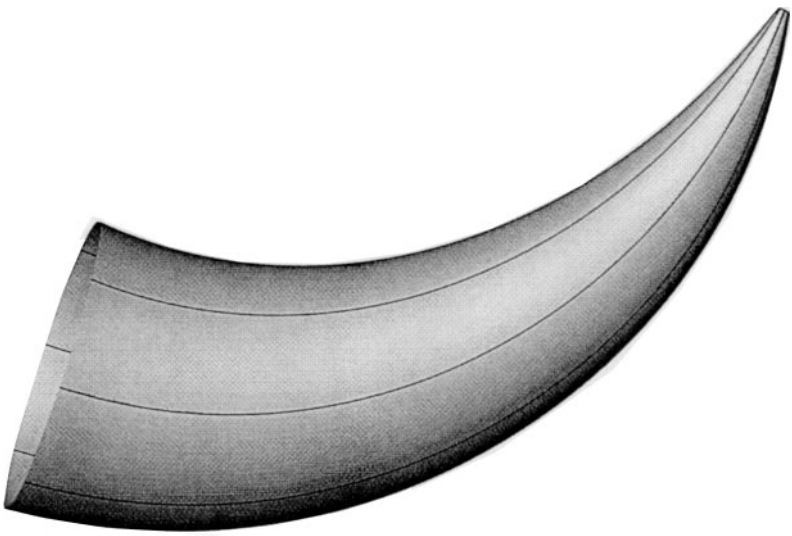

Fig. 15. Computer generated 3-D-view of the horn shown schematically in Fig. 14

The above is sufficient information to develop the full external geometry of the horn. Interior cell tracks are also assumed to be logarithmic spirals in the x_1, x_2 plane and to be connected by circular cross-sections. A 3-D view of this horn generated by a computer program is shown in Fig. 15. The region ADB in Fig. 14 is considered to be part of the skull and is omitted in Fig. 15.

Example 3.8. Horns with 3-D spirals

All of the examples shown in Figs. 5–15 have a plane of symmetry. In this example and in Example 3.9, horns with a three dimensional spiral component will be produced by introducing tangential and asymmetric components of the growth velocity distribution. Here we consider the simplest example of this type of horn or tusk, which is straight but has several screw-like threads similar to the horn of the narwhal. Consider the external form and coordinates shown in Fig. 7. In order to produce spiral cell tracks in the same external form, a rotational component is added to Eq. (34) representing rigid body

rotation about the x_3 axis. Thus,

$$\boldsymbol{v}^g = -\left(\frac{x_1}{t} + \omega x_2\right)\boldsymbol{i}_1 - \left(\frac{x_2}{t} - \omega x_1\right)\boldsymbol{i}_2 + v_0\boldsymbol{i}_3 \,, \tag{55}$$

where ω is the angular velocity. To make the angle of the spiral a constant at the outer surface, ω is varied in time so that

$$\omega = \kappa \frac{v_0}{a} \,, \tag{56}$$

where κ is a constant and a is the maximum radius of G at time t. An example of a tusk with 45° spirals of cell tracks on the outer surface, generated by a computer program using Eq. (55) and $\kappa = 1$ as input is shown in Fig. 16.

It may be noted that although the resultant horn shown in Fig. 16 is unique for the given $\boldsymbol{v}^g$ (Eq. (55)), the decomposition of a given $\boldsymbol{v}^g$ into $\dot{\boldsymbol{x}}^m$ and $\dot{\boldsymbol{x}}^s$ is not unique. In any case, according to Eq. (13),

$$\boldsymbol{v}^g = \dot{\boldsymbol{x}}^m - \dot{\boldsymbol{x}}^G \,. \tag{13}$$

Within the present theory, $\dot{\boldsymbol{x}}^m$ must be a rigid body motion. One choice which is always permissible is $\dot{\boldsymbol{x}}_m = 0$; then $\dot{\boldsymbol{x}}^G = -\boldsymbol{v}^g$.

Another possibility is that G is a fixed surface so that $\dot{\boldsymbol{x}}^G \cdot \boldsymbol{n} = 0$. Then we require

$$\dot{\boldsymbol{x}}^m \cdot \boldsymbol{n} = \boldsymbol{v}^g \cdot \boldsymbol{n} = v_n^g \,, \tag{57}$$

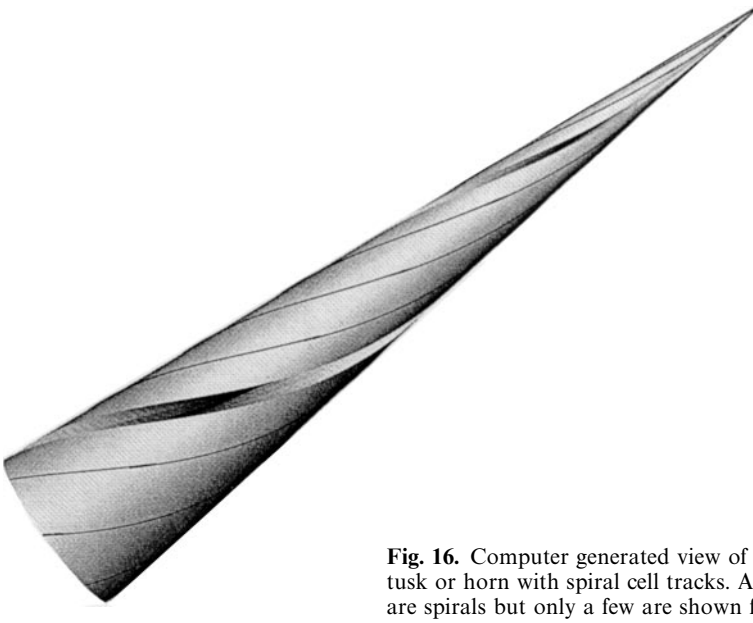

Fig. 16. Computer generated view of a straight tusk or horn with spiral cell tracks. All cell tracks are spirals but only a few are shown for clarity

where v_n^g is the normal component of $\boldsymbol{v}^g$. The tangential component of $\boldsymbol{v}^g$ is $\boldsymbol{v}_t^g$.

$$\boldsymbol{v}_t^g = \boldsymbol{v}^g - v_n^g \boldsymbol{n} \ . \tag{58}$$

There may still be leeway in the choice of splitting $\boldsymbol{v}_t^g$ between $\dot{\boldsymbol{x}}^m$ and $\dot{\boldsymbol{x}}^G$. If $\boldsymbol{v}_t^g$ is not a rigid body motion, then some part of $\boldsymbol{v}_t^g$ must be assigned to $\dot{\boldsymbol{x}}^G$.

In the present case, G is assumed to be the plane $x_3 = 0$ and it is clear that the term $v_0 \boldsymbol{i}_3$ in $\boldsymbol{v}^g$ of Eq. (55) must then be part of $\dot{\boldsymbol{x}}^m$. The terms containing ω in $\boldsymbol{v}^g$ constitute a rigid body rotation which may be assigned to be a part either of $\dot{\boldsymbol{x}}^G$ or of $\dot{\boldsymbol{x}}^m$. If the rotation is assigned to $\dot{\boldsymbol{x}}^G$, then the generating cells would have to rotate around in a circle on G at angular velocity ω and the horn generated would have only a translational velocity v_0 parallel to x_3, similar to Example 3.3. In the present case, the cell tracks would still be spirals.

If the rotation terms in Eq. (55) are assigned to $\dot{\boldsymbol{x}}^m$, then the horn being generated would rotate as it grows. In this case, it follows from Eqs. (55) and (13) that

$$\dot{\boldsymbol{x}}^G = \frac{x_1}{t} \boldsymbol{i}_1 + \frac{x_2}{t} \boldsymbol{i}_2 \ . \tag{59}$$

Equation (59) is a required motion of the generating cells in the outward radial direction on G. This motion is necessary in order that the cell tracks be continuous on the surface of the horn as indicated in Fig. 16. Note that Eq. (59) is equivalent to Eqs. (43) and (44). In Example 3.3 and the present case, the motions of the generating cells are the same, but here the generating cells are inclined at 45° to the normal to G.

Example 3.9. Non-symmetric spiral horns

There are some horns which take a spiral form in space without any plane or axis of symmetry. Such a spiral horn may be visualized as a part of the narwhal's tusk of Example 3.8: the portion of a narwhal's tusk surrounding a particular cell-track forms such a tapered spiral. Consider a circular subdomain G' of radius a_2, centered at a radius a_1 and osculating the circular boundary of G of the Example 3.8 which has radius $a = kt$, as shown in Fig. 17. On G in Example 3.8, the generating cells velocities are

$$\dot{x}_1^G = x_1/t = u_1, \qquad \dot{x}_2^G = x_2/t = u_2 \ . \tag{60}$$

The strain rates in the x_1 and x_2 directions are then

$$\frac{\partial u_1}{\partial x_1} = \frac{\partial u_2}{\partial x_2} = \frac{1}{t} \ . \tag{61}$$

Equation (61) shows that the motion of the generating cells is a spatially isotropic expansion at any time. Hence, the circular domains shown in Fig. 17 remain self-similar for all t. It follows that if Eq. (55) is the assumed growth

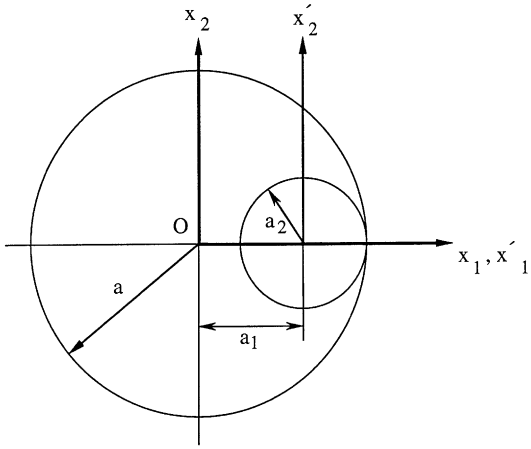

Fig. 17. Growth surfaces for a straight horn (radius a) with spiral cell tracks and a horn which is a spiral in space (radius a_2). The growth velocities are the same for the two cases in the common region (radius a_2)

velocity distribution and G' is restricted to the self-similar circle, $a_2/a = \text{constant}$, as shown in Fig. 17, that from this G', a horn will grow out with spiral cell tracks and the central fiber of horn will also be a spiral in 3-D space.

The above description will produce a spiral horn for which the region G' (of radius a_2) will move in the x_1, x_2 plane. The center $0'$ of G' is at radius a_1, and lies on the x_1 axis. Taking the origin of the moving axes x'_1, x'_2 to be $0'$ i.e. we choose

$$x'_1 = x_1 - \frac{a_1}{a_0} kt, \qquad x'_2 = x_2, \qquad x'_3 = x_3 \; . \tag{62}$$

Then using Eq. (62) to express Eq. (55) yields the growth velocity in terms of x'_i:

$$\boldsymbol{v}^g = -\frac{x'_1}{t}\boldsymbol{i}_1 - \frac{x'_2}{t}\boldsymbol{i}_2 + v_0\boldsymbol{i}_3 + \omega x'_1\boldsymbol{i}_2 - \omega x'_2\boldsymbol{i}_1$$

$$- k\frac{a_1}{a}\boldsymbol{i}_1 + k\omega\frac{a_1}{a}t\,\boldsymbol{i}_2 \; , \tag{63}$$

where ω is again given by Eq. (56). The first two terms in Eq. (63) represent the expansion of G', i.e.,

$$\dot{\boldsymbol{x}}_1^G = \frac{x'_1}{t}\boldsymbol{i}_1 + \frac{x'_2}{t}\boldsymbol{i}_2 \; . \tag{64}$$

The remaining terms of Eq. (63) represent the particle velocity $\dot{\boldsymbol{x}}^m$ relative to the prime coordinates. The next to last term in Eq. (63) is a motion of the horn as a whole in the negative x'_1 direction. This motion is required because the base S'_t and the tip of the horn continually move apart in the x_1 direction. The

last term is a motion in the x_2' direction which gives the cell tracks their orientation.

A spiral horn of an extant antelope is shown in Fig. 18a. A spiral horn generated by a computer program using $\boldsymbol{v}^g$ as given by Eq. (63) is shown in Fig. 18b. The constant ratio (a_1/a) was taken to be 0.9, κ in Eq. (56) was set equal to 1.0, and k/v_0 was set equal to 0.1.

Fig. 18a. Sketches of various extant horn forms (from Bubenik and Bubenik 1990, by permission)

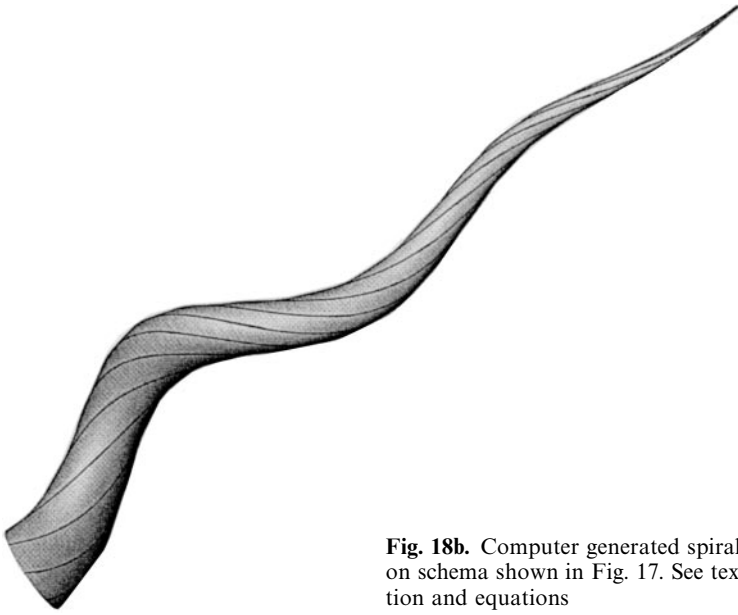

Fig. 18b. Computer generated spiral horn based on schema shown in Fig. 17. See text for explanation and equations

Example 3.10. Antlers

Antlers, in contrast to horns, do not grow at the base, but have the growth surface at the external "velvet" layer; this layer similar to periostial layers that produce the growth of long bones of the skeleton. At the tip of growing antlers there are identifiable layers of the velvet of epidermis, periostium, cartilage and antler bone (Bubenik and Bubenik 1990). Further, there is a blood supply and a neural system. Antler growth is very sensitive to alterations of the neural and endocrine systems which appear to be the major control systems of the growth patterns. From the standpoint of the present paper, the kinematics of antler growth is relatively simple since an external growth surface, G, has little or no kinematic constraint. We may require $\boldsymbol{v}^g$ to be continuous, but any distribution of magnitude and direction is permissible. But the control and spatial guidance systems are complex and not fully understood (see Bubenik and Bubenik 1990, p. 486).

As a simple example of kinematic description of antler growth, consider an antler which starts with a single central shaft which bifurcates to form a terminal fork as shown in Fig. 19A. In the present model, only the formation of the dense cancellous bone layer will be modeled, as shown in the cross-section of Fig. 19B. The interior of the growing antler contains trabecular bone, a blood supply and soft tissues which will not be represented in the present model. At the tip of the growing antler, the main longitudinal growth takes place. In order for a section below the tip to expand in diameter, it is necessary to have some removal of hard tissue from the inner surface of the

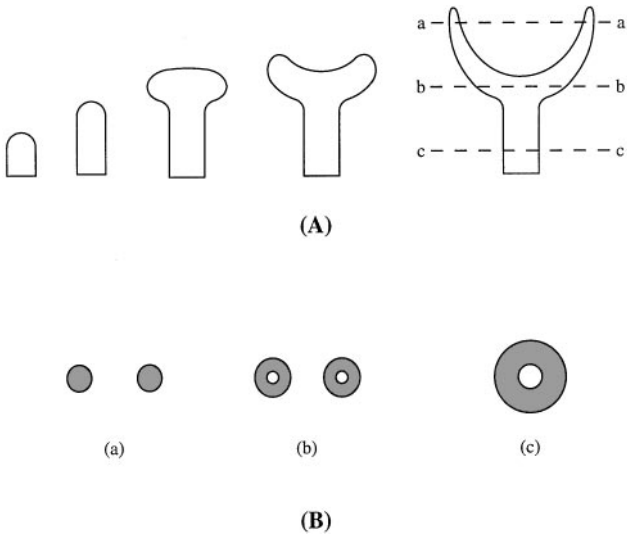

Fig. 19. (A) Schematic diagram of antler growth. The growth surface is always the external surface which expands as the antler grows. (B) Cross-sections of the antler growth shown in (A)

cortical bone to form the nutrient core for further extension of the antler. This is achieved in the present modeling by considering both the inner and outer surfaces of the cortical bone as growth surfaces and specifying an appropriate negative growth velocity on the inner surface.

Since the several layers of the velvet coat on a growing antler are parallel to the external surface of the antler, and growth is predominantly normal to the growth surface (Bubenik and Bubenik 1990). In the computer model, growth is assumed to be normal only so that the entire growth in the model is controlled by specifying the magnitude of the surface growth velocity, $\boldsymbol{v}^g$, as a function of surface coordinates θ_1, θ_2. The growth surface itself is labeled as $\theta_3 = f(t)$, so θ_3 is constant over the entire growth surface at any time. The ranges of θ_1 and θ_2 are held fixed throughout the growth, but the transformation to spatial coordinates

$$x_i^G = x_i^G(\theta_1, \theta_2, t) \tag{65}$$

generates the successive growth surfaces. Bifurcation is produced by reducing the growth rate at the tip point to zero and generating two symmetric centers of growth on either side of it. The resulting bifurcated structure is shown in Fig. 20.

Example 3.11. Turbinate shell

Seashells present a large variety of shapes, which are all grown by a soft tissue called the mantle, which forms a moving growth surface. The forms of

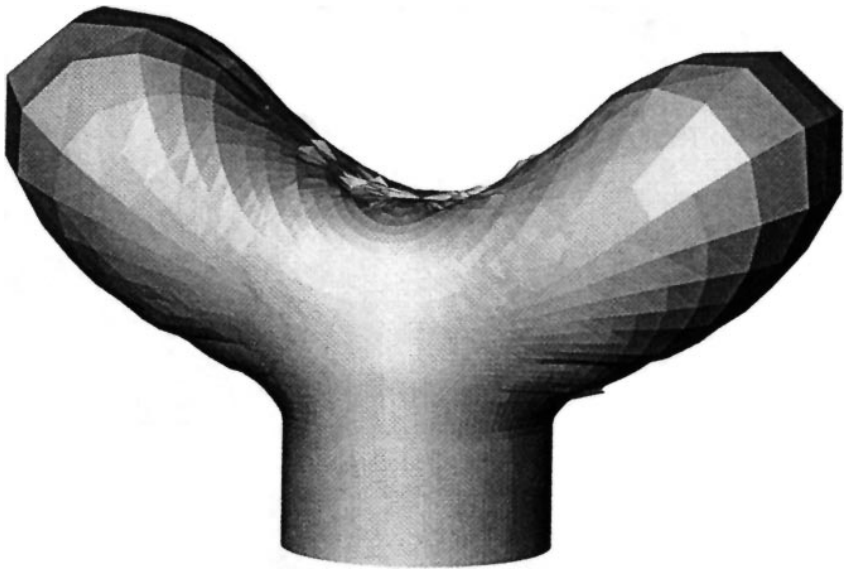

Fig. 20. Computer generated view of a two prong antler produced by surface growth at the external surface. The growth velocity is assumed to be normal to the external surface at every point at all times. The magnitude of the growth velocity is varied in space and time

seashells tend to be self-similar at different ages. This similarity is largely due to the growth velocity being directed at a constant angle, producing logarithmic spirals as cell tracks. The constancy of the spiral angles of several shells and the prevalence of the logarithmic spiral in seashells is extensively documented in D'arcy Thompson's book (1942). Pattern formation on molluscs is discussed by Meinhardt and Klinger (1987).

The self-similarity which results from logarithmic spirals has also formed the basis of computer-generated images which can reproduce many shell shapes. (See Illert 1992a, b for examples and references.) But most such computations have generated only the external surfaces of the sea-shell shapes without the mathematical formulation of growth velocities and computations based directly on the vector growth velocities treated in the present paper. Further, the discussion of cell tracks and the movement of generating cells on the growth surface have not been previously expressed in the mathematical forms of the present paper.

As an example of the growth of a univalve seashell, consider the turbinate shell shown in the sketch in Fig. 21. The generating surface is along the edge of the opening of the spiral. The generating curve is a closed loop whose shape is self-similar as growth proceeds. In general, it need not be plane or a regular shape like a circle or ellipse although it may approximate these. In the case shown in Fig. 21, it is implied the growth surface is plane and always self-similar. The coordinates θ_1, θ_2 have fixed values at corresponding points of the growth surfaces as growth proceeds, and each growth surface has

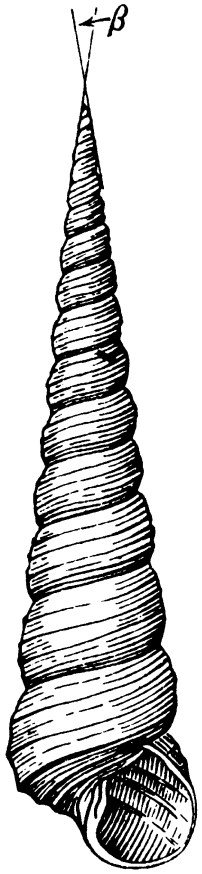

Fig. 21. Sketch of a univalve turbinate shell. (From Dárcy Thompson 1942, by permission)

a constant θ_3. The successive growth surfaces H_τ may be seen as faint ridges or color markings on many shells. They are called "generating curves" by D'arcy Thompson (1942) and he calls each line with $\theta_1, \theta_2 =$ constants, a generating line or generating spiral. These are called cell tracks here.

The self-similar shell form is produced by holding the angle of the growth velocity, $\boldsymbol{v}^g$, constant at each point of the growth surface, i.e. at each $\theta_1, \theta_2 =$ constant. The angle of $\boldsymbol{v}^g$ is constant in the sense that the angles it makes with a normal vector to G and with the axis of the shell are constant. The magnitude of $\boldsymbol{v}^g$ at each point of the growth surface is adjusted so that relative to G, the shell has a rigid body motion. Figure 22 shows a turbinate shell generated by a computer program using these guidelines.

Example 3.12. Bivalve shell

In bivalves, such as clams, oysters, and scallops, there are two growth surfaces, one on each leaf of the shell on the plane or curve on which the leaves meet.

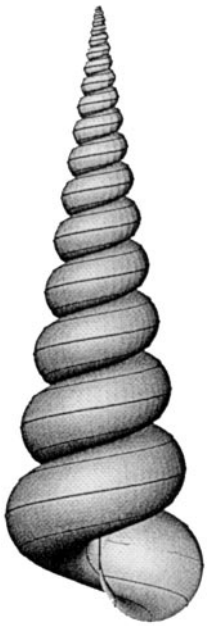

Fig. 22. Computer generated turbinate shell. See text for assumptions of growth velocity directions and magnitudes. The spiral lines shown are computer generated cell tracks

Bivalves tend to be self-similar in form at different ages and it follows that the cross-sections are approximately logarithmic spirals as discussed by D'arcy Thompson (1942). A sketch of a bivalve, Cardium edule, is shown in Fig. 23. In this sketch, the current growth surface is called a directing curve and earlier growth surfaces are called incremental lines. The cell tracks are called "costa" and are generally curved, but are quite straight near the central section. As shown in Fig. 23C, the cross-section along a straight cell track is close to a logarithmic spiral. The angle α (Fig. 10) is relatively small in bivalves, and only a small portion of one complete turn of the spiral is traversed in a complete shell.

The self-similar form of a bivalve shell is produced mathematically in the same fashion as a univalve. The growth surface is always self-similar and has the same range of θ_1, θ_2 while it expands and rotates in x_i space. At each point $\theta_1, \theta_2 =$ constant, the angles that $\boldsymbol{v}^g$ makes with the normal to G and to the hinge axis (Fig. 23A) are held fixed with respect to time. The magnitude of $\boldsymbol{v}^g$ at each point of the growth surface is adjusted so that relative to G, the motion of the shell is that of a rigid body. Figure 24 shows a bivalve shell generated by a computer program using these rules. In Fig. 24, the edge of the growth surface was taken to be a smooth curve. The cell tracks then generate a smooth surface like a clam. Production of ridges such as the cell tracks shown in Fig. 23 requires the growth surface edge to be serrated and to preserve these serrations as the shell grows. The growth in the surface G needs only to be isotropic, which automatically preserves the general form as well as the details of the raised cell tracks (costa).

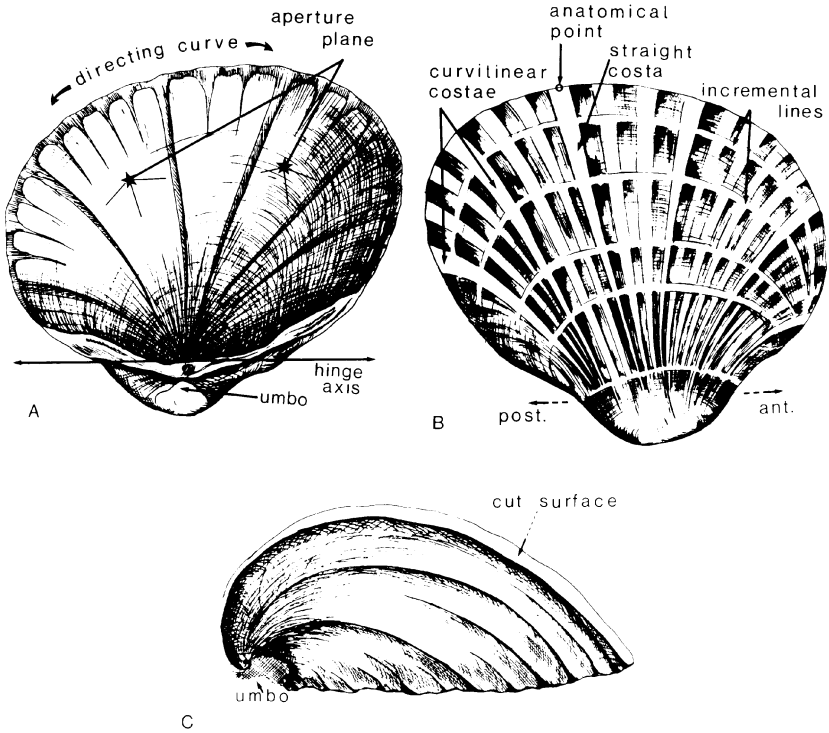

Fig. 23. Sketches of one leaf of a bivalve (cardium edule). (A) The "directing curve" is the current growth surface. (B) The "costa" follow cell tracks. The "incremental lines" are previous growth surface H_τ. (Fig. 1B). (C) The cross-section is a logarithmic spiral. (From Vilmann et al. 1981, by permission)

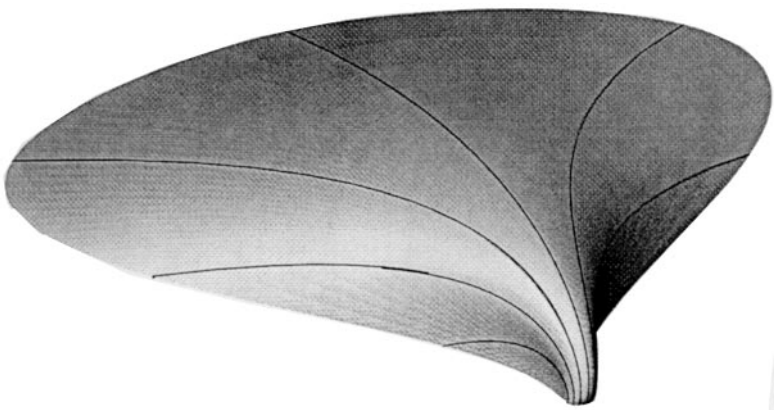

Fig. 24. Computer generated view of a model of a bivalve leaf similar to the sketches in Fig. 23. All cell tracks are logarithmic spirals with the same constant angle α (Fig. 10)

Example 3.13. Teeth

The growth of teeth represents a general category of surface growth in which two growth surfaces, which start from the same surface, grow outward and inward from the initial surface. The inward-growing surface deposits dentin and the outward growing surface deposits enamel, as shown in the sketch of the tooth cross-section in Fig. 25. Enamel has a distinct prism structure, each prism having been formed by one cell (ameleoblast) so prisms are, in fact, cell tracks. The prisms run approximately normal to each growth surface, but there are some undulations. Prisms run parallel to each other in bands (Hunter–Schreger bands), but the bands decussate with adjacent bands in the inner third of the enamel. The growth surfaces at various stages (called H_τ in Sect. 2, above) are known as incremental lines in enamel or the lines of Retzius. The discussation (crossed orientations) of successive layers may improve the fracture toughness and is found in the structure of seashells also. In the present vocabulary, the existence of discussating layers implies that the angle which $\boldsymbol{v}^g$ makes with the tangent plane to the growing surface of the tooth varies at the scale of prisms of enamel, which are basically at the cellular level. In the computer model of a tooth shown in Fig. 26, the undulation of the growth velocity $\boldsymbol{v}^g$ and the resultant Schreger lines are not represented; Schreger's

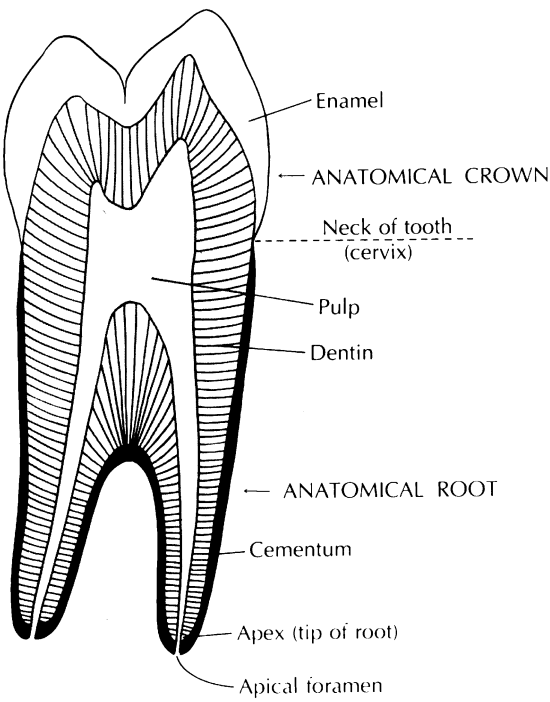

Fig. 25. Diagram of a section through the entire length of a human tooth (premolar). (From Moss-Salentijn and Hendricks-Klyvert 1990, by permission)

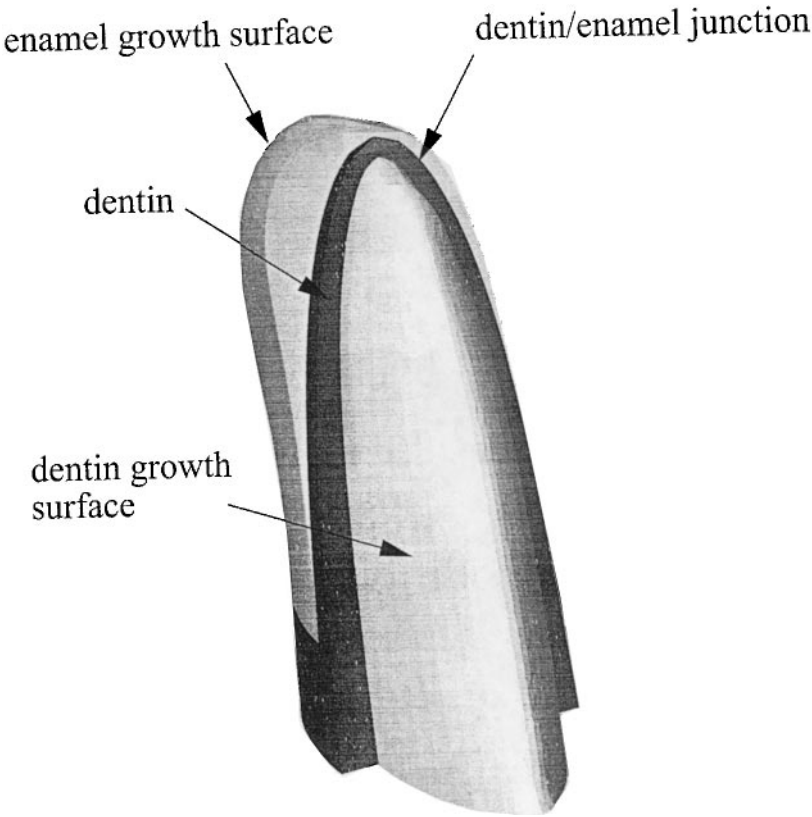

Fig. 26. Computer simulation of the growth of the crown of a tooth (incisor). The enamel and dentin arise from opposite sides of a common surface. The growth of both the enamel and dentin is assumed to be normal to their growth surfaces

lines could be generated by this model by including a very fine variation of direction of $\boldsymbol{v}^g$.

The cell tracks (generated by odontoblasts) in dentin, which grows inwards from the initial growth surface (interlobular space of Owen), are also primarily normal to the growth surface as indicated by the striations in Fig. 25. The growth surfaces at various times (H_τ) can be observed in sections of teeth and are called contour lines or lines of Owen.

A computer simulation of a growing tooth is shown in Fig. 26 in which $\boldsymbol{v}^g$ has been adjusted so that $\boldsymbol{v}^g$ is always parallel to the normal to the current growth surface both on the dentin growth surface and the enamel growth surface to arrive at the cell tracks similar to those in Fig. 25. The magnitude of $\boldsymbol{v}^g$ is varied in time and space to produce the changing forms as growth proceeds. The initial growth surface for dentin and enamel is the common growth surface G_0 (interlobular space of Owen). On this surface, θ_1 and θ_2 values are assigned and the growths of dentin and enamel are modeled as

two separate growth sequences, so that surfaces $\theta_3 = \tau$ are a pair of surfaces, H_τ, one in enamel and one in dentin which locates the growth surfaces which existed simultaneously at time $t = \tau$.

4 Residual stress due to surface growth

In the theory of Sect. 2 and the examples of Sect. 3, it is assumed that the surface growth considered is compatible and causes no residual stress. The meaning or definition of compatibility, in the case of a general surface growth, is not explicitly discussed in the usual continuum mechanics literature and also does not fall within the discussion of compatibility of volumetric growth (Skalak et al. 1995). The question to be answered can be stated as follows: Given a growth surface, G, and a growth velocity distribution $\boldsymbol{v}^g$ on G, what conditions should G and $\boldsymbol{v}^g$ satisfy to qualify as a compatible surface growth? The physical ideas of compatibility may be regarded as analogous to the requirements of 3-D elasticity: The growth should not create any holes, tears, overlaps and should not cause residual stresses. The problem is to translate these ideas into mathematical criteria.

The definition of compatibility for surface growth as stated above is not directly comparable to the usual discussion of compatibility in the theory of elasticity, where conditions on a proposed strain field are sought in order to have a single-valued displacement field. The compatibility of surface growth could be discussed in analogous terms, i.e., under what conditions of a surface strain field on G, does a single valued displacement of G exist? This level of the discussion is avoided here by assuming that $\boldsymbol{v}^g$ is a continuous velocity distribution postulated to exist a priori. The compatibility of growth strains within G may be a separate question of some interest, but does not correspond to the entry level of the discussion posed here.

Consider first the case of surface growth on an external surface such as in the growth of antlers. The normal component of $\boldsymbol{v}^g$ specifies a local rate of mass accretion (Eq. (29)). Assuming the new material is deposited in an unstressed condition, there does not appear to be any mechanism to cause residual stress. However, if the newly added material is somehow made to shrink or expand after it is placed, then residual stress may be induced. Such cases will be discussed later in this section.

In the cases of external surface growth, such as in antlers or seashells, the tangential component of $\boldsymbol{v}^g$ (tangential to G) may be ascribed to motion of the generating cells, assuming that the growing body itself is fixed in space, as explained in Sect. 2 and illustrated in the examples of Sect. 3. Thus, it appears that if $\boldsymbol{v}^g$ is a continuous vector field over any continuous G which is an external surface, then no further requirements need be placed on $\boldsymbol{v}^g$ for compatibility.

A more obvious and direct way that surface growth may induce residual stresses can occur when the surface growth takes place on an internal surface such as at the base of growing horn. In the horn Examples 3.1–3.9 discussed in

the previous section, the growth velocities $\boldsymbol{v}^g$ assumed were compatible with rigid body motions of the horns relative to the skulls which were also considered to be rigid. As long as the growth velocities $\boldsymbol{v}^g$ are compatible in this way, no residual stress is necessary. Residual stresses will be necessary if at some point, the growth velocity $\boldsymbol{v}^g$ on G is not compatible with a rigid body motion of the horn relative to the skull. To postulate a specific example, consider the Example 3.1 again in which the growth velocity is assumed to be a uniform vector over G (Eq. (30)). Suppose that after some time, the growth velocity changes so that for a period from t_1 to t_2 the growth velocity is

$$\boldsymbol{v}^g = v_0\left(1 + b\cos\frac{\pi r}{2a}\right)\boldsymbol{i}_3 \ , \tag{66}$$

where r is the cylindrical coordinate and b is a constant. After time t_2, it is assumed the growth velocity $\boldsymbol{v}^g$ reverts to Eq. (30). Since the growth velocity $\boldsymbol{v}^g$ given by Eq. (66) is not compatible with rigid body motion, residual stresses will be required to maintain the continuity of the horn and skull. The problem to be solved to find the residual stresses is illustrated in Fig. 27. The uniform growth up to time t_1 is shown in Fig. 27A. For a time t during the interval $t_1 < t < t_2$, the uninhibited growth assumed (Eq. (66)) would produce the incompatible parts shown in Fig. 27B. Residual stresses are required to maintain continuity of the horn and skull as shown in Fig. 27C. In the problem posed in Fig. 27, residual stresses are required beginning at $t = t_1$ and they will be changing with time thereafter due to the continued incompatible growth.

In the above discussion, it is assumed that the cells producing growth are capable of producing the assumed growth velocity $\boldsymbol{v}^g$, Eq. (66) against the influence of the residual stresses that such incompatible growth produces. In real life it may be expected that such residual stresses will influence the rate of growth and tend to force it into a compatible mode.

In summary, a compatibility rule for surface growth on an interior surface may be stated as follows: A vector field of surface growth $\boldsymbol{v}^g$ is compatible on an interior surface G if $\boldsymbol{v}^g$ is of the form of a Volterra dislocation, i.e. Eq. (21). In this case, the relative motion of the two parts of the body, either side of the growth surface, are rigid body motions.

It is also possible to generate an incompatibility due to tangential components of $\boldsymbol{v}^g$ if cells on G and G itself are assumed to be fixed in location, but there are tangential components of $\boldsymbol{v}^g$. For example, a radial outward component of $\boldsymbol{v}^g$ as given in Example 3.3 (Fig. 7) by Eq. (34) would be incompatible if $\dot{x}_i^G$ were assumed to be zero instead of the result given by Eqs. (43) and (44).

A general rule may be given in the case that it is assumed that G is fixed and the growth-producing cells are fixed in location on G. As already discussed in Sect. 2, the entire growth velocity field $\boldsymbol{v}^g$ on G must have the form of a Volterra dislocation, Eq. (21).

Returning now to the possibility of residual stresses being produced by contraction or expansion of tissue after it is deposited on an external surface

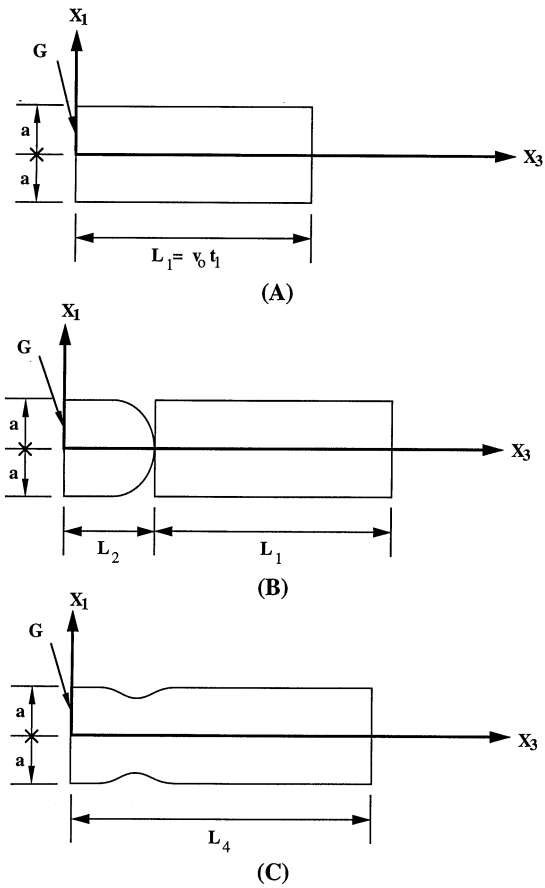

Fig. 27. Schematic illustration of origin of possible residual stresses due to surface growth. (A) Uniform growth without residual stresses up to time $t = t_1$. (B) Incompatible growth due to non-uniform surface growth, assuming no residual stresses. (C) Resulting shape if residual stresses are assumed to maintain compatibility of the growing structure

G of a growing body, it may be remarked first that this is not a surface growth phenomenon. The proposed expansion or contraction of tissue after it is placed, falls under the general category of volumetric growth which is treated in a previous paper (Skalak et al. 1996). This case is mentioned here because it may be biologically important and may, in fact, be taking place only in a thin layer near the surface of a body. If a thin surface layer on any solid body contracts or expands without growth or atrophy in the interior of the body, it may be expected that residual stresses are produced.

An example of residual stress induced by contraction of surface growth may be found in wound healing. Some tissue is laid down and then it is contracted to form a scar tissue and induces tension in the surrounding skin.

Another possible example is the origin of residual stress in the walls of arteries, which are known to have large residual strains in vivo in both the

circumferential as well as longitudinal directions. As such arteries grow or hypertrophy due to elevation of blood pressure, or normal growth through childhood, it may be that the new tissue is laid down first and then contracts rather than being laid down under the final prestress. These possibilities need experimental information to verify the actual mechanisms.

5 Discussion and conclusions

The present paper is intended to supply a rigorous vocabulary for the description of various kinds of surface growth and to illustrate the use and results of this vocabulary in some common cases of horns, seashells and teeth. This vocabulary is on one hand rigorous and on the other hand flexible; it covers the possibilities of fixed or deforming growth surface and the definition of surface growth velocity is independent of the coordinates chosen. They may be assumed to be fixed relative to the growth surface or to the body being generated.

A unique feature of the present treatment is that the surface growth velocity is assumed at the outset to be either inclined to or perpendicular to the current growth surface. This allows generation of space-curved structures such as a spiral horn, without requiring rotation of the growth surface itself. In the present theory, it is assumed that all the growth is produced by cells which are aligned parallel to the growth velocity vector. This is not essential to the theory presented here, but provides motivation for it. This assumption, as well as the actual motion of growth cells within the growth surface, needs to be verified in any particular biological case.

The present paper does not provide any biological proof that the descriptions provided apply to any particular biological case. Rather, a rigorous vocabulary is presented and it remains to be seen by biological observations and experiments, where such theory does not provide a realistic description. Of course, in many cases there are observations recorded in the literature which assure that many of the aspects of the examples presented here are realistic. For example, it is known that the rhinoceros horn is matted hair, and hence, it has cell tracks more like Fig. 6 than Fig. 7. On the other hand, the structure of cows' horns is known to be more like Fig. 7.

There are two points of the present vocabulary that particularly need to be confirmed or verified in each biological case. The first is the extent to which cell tracks (like the costa of Fig. 23) are, in fact, attributable to a single cell or to a group of cells, in which individual cells divide or die and are replaced by new cells.

The second aspect which requires experimental information is the nature and degree of motion of generating cells. (This is the velocity called $\dot{\boldsymbol{x}}^G$ in Eq. (12).) If the surface supporting the generating cells is bone and the growth of the supporting structure is the reason for the motion of the generating cells, one possibility is that there is an isotropic growth of the growth surface G and its supporting structure. Then no residual stresses

are required. In the examples shown in Figs. 6–24, only such isotropic base growth is required.

The motion of the generating cells (or its equivalent), may also be produced by the deformation of soft tissue in which the generating cells reside. This may be the case for the growth of a whelk shell which has series of periodic bumps or protrusions on its outer spiral. These must be produced by corresponding variations of the growth surface G as the shell grows. The true marvel of surface growth, is the control system which must regulate such undulations in this case and such complexities as 10-point antlers, or the composite curves of spiral horns. The present paper does not consider these control mechanisms, but may provide a rigorous kinematic vocabulary for their discussion.

Acknowledgements. The authors are grateful for useful discussions with and the advice of Professors Melvin L. Moss, Letty Moss-Salentjin, and Rakesh K. Jain. Funding for research was provided partially by NSF PYI Award CMS 90-57629 and NIH Grant HL43026.

References

Bubenik, G. A., Bubenik, A. B. (eds.): Horns, pronghorns and antlers. New York: Springer 1990

Cowin, S. C.: Bone stress adaptation models. J. Biomech. Eng., **115**, 528–533 (1993)

Fawcett, D. W.: A textbook of histology, 12th Edn. New York: Chapman & Hall 1994

Gierer, A.: Generation of biological patterns and form: some physical, mathematical, and logical aspects. Prog. Biophys. Molecular Biol. **37**, 1–47 (1981)

Huiskes, R., Hollister, S. J.: From structure to process, from cell to organ: developments of F-E analysis in orthopedic biomechanics. J. Biomech. Eng., **115**, 520–527 (1993)

Illert, C.: Foundations of theoretical conchology. Palm Harbor, FL: Hadronic Press 1992a

Illert, C., Pickover, C. A.: Generating irregularly oscillating fossil seashells. IEEE Comput. Graphics Appl. **12**, 18–22 (1992b)

Koch, A. J., Meinhardt, H.: Biological pattern formation: from basic mechanisms to complex structures. Rev. Mod. Phys. **66**, 1481–1507 (1994)

Meinhardt, H., Klinger, M.: A model for pattern formation on the shells of molluscs. J. Theor. Biol. **126**, 63–69 (1987)

Moss-Salentijn, L., Hendricks-Klyvert, M.: Dental and oral tissues: an introduction. 3rd Edn. Philadelphia: Lea & Febiger 1990

Mullender, M. G., Huiskes, R., Weinans, H.: A physiological approach to the simulation of bone remodeling as a self-organizational control process. J. Biomech. **27**, 1389–1394 (1994)

Murray, J. D.: Mathematical Biology. Berlin: Springer-Verlag 1989

Nicolis, G., Prigogine, I.: Self-organization in nonequilibrium systems. New York: Wiley 1977

Skalak, R.: Growth as a finite displacement field. In: Proc. IUTAM Symp. on Finite Elasticity. Netherlands: Martinus Nijhoff, The Hague 1981

Skalak, R., Zargaryan, S., Jain, R. K., Netti, P. A., Hoger, A.: Compatibility and the genesis of residual stress by volumetric growth. J. Math. Biol. **34**, 889–914 (1996)

Thompson, D. W.: On growth and form, 2nd Edn, Vols. I and II. Cambridge, UK: Cambridge University Press 1942

Turing, A. M.: The chemical basis of morphogenesis. Philos. Trans. Roy. Soc. London Ser. B **237**, 37–72 (1952)

Vilmann, H., Moss, M. L., Skalak, R., Vilmann, O.: Space–time presentations of the shell of the bivalved mollusk cardium edule. Am. J. Orthod. **80**, 417–428 (1981)